

Article

Water Stress Index detection using a low-cost Infrared sensor and Excess Green Image processing

Rodrigo Leme de Paulo¹; Angel Pontin Garcia¹; Claudio Kiyoshi Umezu¹; Antonio Pires de Camargo¹; Fabrício Theodoro Soares¹; Daniel Albiero^{1*}

¹School of Agricultural Engineering, University of Campinas, Campinas-Brazil, ZIPCODE: 13083-875. Brazil (Tel: 55-19-3521-1024,

rodrigolemepaulo@gmail.com, angelpg@unicamp.br, umezu@unicamp.br, apcpires@unicamp.br, ftsoares@outlook.com, daniel.albiero@gmail.com

*Corresponding author: daniel.albiero@gmail.com

Abstract: So that the levels of water stress are not harmful to the development of the crop and affect its productivity, its detection and monitoring are necessary, and it can occur in different ways. One of them is through the Crop Water Stress Index (CWSI). This index quantifies water stress through the normalization of leaf temperature between the maximum and minimum plant temperatures as a function of evaporation conditions. The responses of a low-cost infrared (IR) sensor were crossed with image processing through segmentation by the Excess Green model to develop a water stress detection system using CWSI. A soil/plant temperature map was generated through a point-to-point scan of the IR sensor. And when it overlaid with a segmented image of the experimental area, only points identified as plants had their temperature values maintained. The Non-Water-Stressed Baseline (NWSB) equation was parameterized for the same conditions of the experiment and external environmental. The experimental area was divided into three different treatments, maintained under stable water conditions throughout the experiment and the system was able to identify stably different stress values between treatments. Although the relationship between crop and environment affected the results, this work showed that using an irrigation system based on CWSI is possible.

Keywords: Water Stress; Precision Irrigation; Non-Water-Stressed Baseline; Soil Moisture; Infra-Red Sensor.

1. Introduction

The detection of water stress is vital in Precision Irrigation (PI) management to ensure that plants are not subjected to stress levels that excessively restrict productivity or even production quality [1–3]. Among the ways to detect water stress, methods that measure soil water tension, stomatal conduction potential, and sap flow stand out [4,5]. Soil water tension indicates the energy with which water is retained in the soil matrix and is, therefore, an indirect measure of the water stress to which the plant is subjected [6]. On the other hand, the stomatal conduction and sap flow methods are not very applicable in the field since they are destructive tests and require specific instrumentation [7,8].

Under water stress conditions, there is stomatal closure, reduced transpiration, and a consequent increase in leaf temperature concerning ambient temperature. The Crop Water Stress Index (CWSI) makes it possible to quantify the stress level by normalizing leaf temperature between the maximum (when there is no evaporation) and minimum plant temperatures (when evaporation is at its maximum potential). Kacira et al., (2002) detected water stress in flowers, identifying a quick response of this method, anticipating the identification by up to 2 days, compared to conventional methods, showing the advantage of using this index. In a simplified way, the CWSI can be calculated based on the

difference between leaf (T_F) and ambient (T_A) temperatures, as shown in Equation 1.[6] Initially, the plant's canopy temperature (T_C) is considered, but in this work, it was considered T_F by the size of the crop evaluated.

$$CWSI = \frac{(T_F - T_A) - (T_F - T_A)_{LL}}{(T_F - T_A)_{UL} - (T_F - T_A)} \quad [\text{Equation 1}]$$

Where $(T_F - T_A)_{LL}$ e $(T_F - T_A)_{UL}$ are the upper and lower limits, found by the *Non-Water-Stressed-Baseline Equation* (NWSB). It is specific for each crop and correlates the difference between leaf temperatures and the environment with the vapor pressure deficit (VPD) [9].

The literature on the CWSI is relatively vast. And studies focus on ways to obtain the index [7,10,11] in evaluating the behavior of crops concerning the CWSI[12–15] and in the ways to use the information in irrigation management systems [16–18]. All these studies have in common the use of similar methodologies for data acquisition, such as the use of infrared temperature sensors (IR) and thermal cameras to obtain the leaf temperatures of plants. However, in small-scale applications, the high cost of thermal cameras can be a limiting factor for getting thermal maps, and IR sensors can be a technically viable and lower-cost alternative.

This work aims to develop a water stress detection system using leaf temperature index, obtained by crossing the responses of a low-cost infrared sensor with image processing through segmentation by the Excess Green model.

2. Materials and Methods

The work was carried out at the Instrumentation and Control Laboratory of the School of Agricultural Engineering (LIC/FEAGRI), in the city of Campinas, SP, Brazil (22°49'08.60S 47°03'38.37"W). A Farmbot (FARMBOT,2021) was used, an open-source gantry robot with a customized interface built in LIC/FEAGRI. Thus, it is possible to couple sensors and equipment for monitoring and control of tillage conditions.

The tillage area of the test bench is 0.75m x 1.50m x 0.25m, where arugula (*Eruca sativa miller*) was cultivated in the spacing of 0.20m between rows and 0.05m between plants, according to the recommendations by [19]. Vegetable land was used as a growing medium for the plants. Arugula was chosen for the experiments because of its ease of cultivation and homogeneous distribution of leaf shape. Figure 1 illustrates steps of the adopted methodology: (i) acquisition of temperature, relative humidity, and plant height data; (ii) image acquisition and processing, (iii) reference thermal image acquisition, (iv) parameterization of the NWSB equation, (v) soil moisture monitoring.

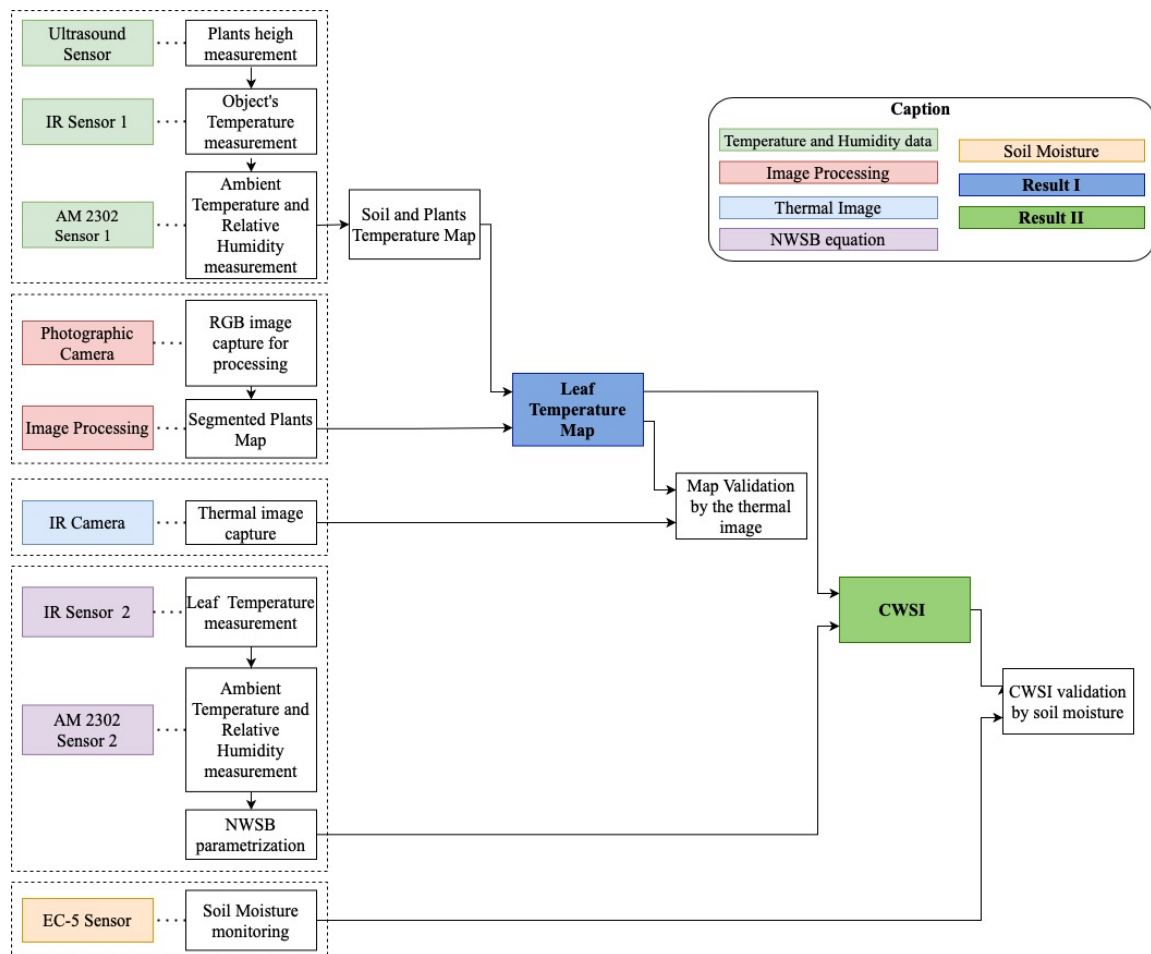


Figure 1 – Steps of the methodology adopted for detection of water stress through the CWSI.

Instrumentation and equipment used

The bench was instrumented with infrared, ultrasound, temperature, and humidity sensors and an optical camera. Figure 2 shows the system's configuration in which the tests were performed, with the sensors and embedded devices for data processing.

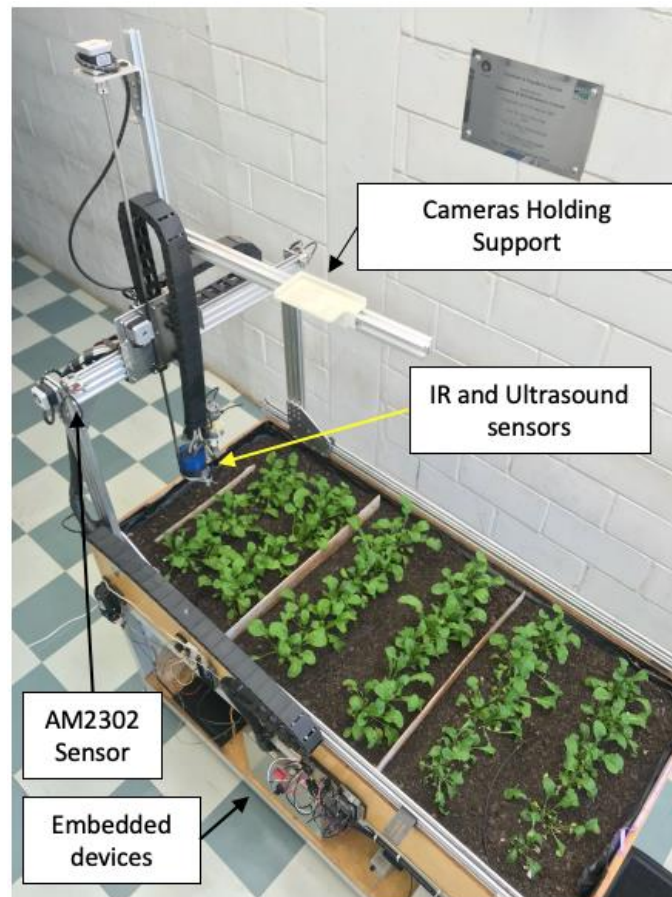


Figure 2 - Schematic of the bench test, showing the arrangement of sets of sensors to detect water stress through CWSI.

Plant height monitoring was performed using a digital ultrasound sensor model HC-SR04, with an operating range between 2mm and 4m and ± 3 mm precision. Literature mentions that the distance between the temperature sensor and the leaf surface influences the measurement quality. Therefore, the vertical distance adopted was 0.05 m to improve the quality of temperature determinations in this project, considering the small size of the arugula. The adopted distance was also used for the crops of lettuce [20], saffron [21], black pepper [13] and the results obtained by these studies showed that temperature readings at this distance were adequate for monitoring plant water stress.

The IR sensor used in this experiment was the MLX90614-ESF-BAA, manufacturer Melexis, with an operating range between -70 e 180°C , $\pm 0.5^{\circ}\text{C}$ precision, and 90° conical field of view (FOV) with the emissivity of the adjustable sensor between 0.00 and 1.00. In the experiments, the equipment was regulated to capture the emissivity of vegetable leaves equal to 0.98 [22,23]. The temperature measured by the IR sensor also called the Object Temperature (T_o), is the mean of all temperatures within the reading area. As the FOV is conical, its reduction will decrease the reading area and, therefore, it will present a more accurate reading, since both are directly proportional. A metallic apparatus was used to reduce the FOV in the sensor that collimates the infrared beam. Since the IR sensor reading area is a function of the height of the set of the sensor set, this must be kept constant [24].

Sensor AM2302, manufacturer Aosong, was used to measure TA and RH in an operating range between -40 to 80°C and 0 to 100%RH, precision $\pm 0.5^{\circ}\text{C}$, and $\pm 2\%$ RH. This sensor is widely used for its precision and ease of communication with embedded devices[25–27].

The IR camera for obtaining the thermal reference images was the FLIR B400 from the manufacturer FLIR Systems, calibrated and certified in October/2019, with an operating range between -100 and 350°C , sensitivity from 0.05°C to 30°C , and 2% precision. The iPhone 7 digital camera (Apple Inc.) was used to obtain the RGB images with the

specifications: 1/3" sensor with 12MP resolution, f/1.8, 28mm, and optical image stabilization set. Capacitive sensors were used to monitor soil moisture, model EC-5, Decagon Devices, with a measuring range from 0 to 0.60 m³ m⁻³, a precision of 0.02 m³ m⁻³.

Leaf Temperature Map (MTF)

The difference between leaf (T_F) and ambient (T_A) temperatures is one of the parameters used in the CWSI equation. Information from the thermal map generated by the IR sensor was crossed with the image of segmented plants to create a Leaf Temperature Map, where only the plants were considered. The image resulting from the segmentation was converted into a binary mask, where the segmented points of the plant have a value equal to 1 and the other points equal to 0. Thus, the thermal map selective was obtained by applying the generated mask on the thermal map, preserving only plant temperatures.

Soil/Plant Thermal Map

The Farmbot uses stepper motors to move the set of sensors three-dimensionally along the X, Y and Z axes. Using local coordinates, the pack ran through the entire test area, performing a daily pre-scan with a fixed height of 0.5m above ground level to determine the plants' height range through the ultrasound sensor. Then, according to the maximum size obtained, the height of the set was adjusted so that the infrared sensor reading was 0.05m above the plants level. The distance of the set was measured with the aid of a measuring tape.

A daily scan was performed, taking static readings of information from IR sensors and air temperature and humidity throughout the growing period, always at 12:00 pm. This time presented the best correlation between CWSI and leaf water potential (Y_L) [28]. A pixel with a size of 20x20mm was established where, at each point, the X, Y coordinates and the T_O values were known, in addition to the T_A and RH at the time of reading. It is worth mentioning that the information was read in places with plant and soil, only plant or only soil, according to their location. Therefore, it was possible to generate a Soil/Plant Thermal Map of the experimental area with the T_O information. At the same time, the other two parameters read were used to calculate the CWSI.

Image processing

Computer vision techniques were applied for the identification and segmentation of leaves and soil. The tests were carried out with the RGB camera and a computer with a 3.90GHz 8th generation Intel Core i5 processor, 12GB of RAM and a 2GB NVIDIA GEFORCE MX 130 video card. The algorithm for image processing was built in PYTHON language and used the following libraries: *Open-CV* for commands related to image manipulations; *Numpy* for the realization of the mathematical operations involved in the process; and *Pandas* for grouping and organizing the output data (*outputs*). The ExG(RGB) model was used for image segmentation ([29], previously evaluated as the model that presented the best performance indices under the conditions of the experiment.

During the cultivation cycle, 15 images were taken in the same position perpendicular to the bench. Segmentation quality was quantified by the F-score [30,31]. The *F-score* is defined as the harmonic mean between precision (number of correct positive classifications concerning the total positive classifications) and sensitivity (number of correct positive classifications about pixels belonging to plants). This metric quantifies the classification of images robustly between the absence of True Positives (TP) as 0 and a perfect classification as 1. In addition, the data were also evaluated using descriptive statistics.

The images that served as a reference to determine whether the classification was correct or not were manually classified. The binarization of each image was done through the mean of 10 pixels selected using the RGB values of the plants. Pixels within the range of values between $Mean \pm standard\ deviation$ were considered plant (value 1) so that pixels containing soil received a value of 0.

MTF Validation

The overlapping of the segmented image on the Soil/Plant thermal map generated the MTF, used to calculate the CWSI. Its evaluation was made by comparing it with the image generated by the IR camera, which was positioned perpendicular to the ground. According to the literature, the measurement distance was also 1m. The thermal images obtained by the IR camera were processed by the manufacturer's software. The validation was done by analyzing pixel by pixel, by the difference between the temperatures read by the IR sensor ($S_{x,y}$) and by the camera ($C_{x,y}$), as shown in Equation 3 and the general mean error calculated by Equation 4, where n is the number of pixels of the generated maps. In addition, the mean standard error was also calculated.

$$Error_{x,y} = \frac{S_{x,y} - C_{x,y}}{C_{x,y}} \quad [\text{Equation 3}]$$

$$\text{General mean error} = \frac{\sum error_{x,y}}{n} \quad [\text{Equation 4}]$$

Parameterization of the Non-Water-Stressed Baseline (NWSB)

The NWSB equation was parameterized with data obtained from a second experimental bench, with characteristics equal to the principal bench, such as the same dimensions, soil type, quantity, and plants spacing. In addition, the two benches were located in the same environment, enabling the sharing of data and conditions.

A second AM2302 sensor was used to take the T_A and RH readings, and another IR sensor, arranged at fixed points to read the T_F of the plants. It is essential to highlight that as this sensor did not perform a scan but fixed readings, it was positioned so that only the arugula leaves were within the sensor reading area, as did [28].

Measurements were taken with an interval of 10 minutes for 30 days, corresponding to the arugula cultivation cycle. Therefore, in addition to considering two planting cycles for the parameterization of the equation, it was necessary to calculate the vapor pressure deficit (VPD) (Equation 5) through the T_A e RH values read by the AM2302 sensor.

$$VPD = (1 - UR) * 0,6108 \cdot 10^{\frac{7,5T_A}{273,3+T_A}} \quad [\text{Equation 5}]$$

By correlating the values of $(T_F - T_A)$ and VPD, the NWSB equation corresponds to the linearized model of the set of generated points. Therefore, this equation was used to calculate the water stress of plants on the principal test bench. Following [32] methodology, $(T_F - T_A)$ and the VPD could be correlated according to the time of measurements, as they vary throughout the day. However, we chose to use a simplified correlation and only a daily mean value for this study since scanning the points and calculating the CWSI were performed only once a day. The curves obtained by these correlations provided the NWSB equations.

The lower limit $(T_F - T_A)_{LL}$ of the CWSI was calculated using the NWSB equation, with the VPD values of the environment at the time of reading during the daily scan of the sensors, which can be understood as the linear coefficient of the equation obtained. The upper limit $(T_F - T_A)_{UL}$ calculation followed the methodology used by [33]. This methodology uses a potential VPD to simulate the increase of $(T_F - T_A)$ when the VPD is zero at ambient temperature, generating a new value of VPD that must be used in the NWSB equation, resulting in the maximum limit of the temperature difference.

CWSI Calculation

It was possible to calculate the CWSI by Equation 6 with all parameters defined, quantitatively finding the degree

of stress of the plant at the moment of the scan.

$$CWSI = \frac{(T_F - T_A) - (T_F - T_A)_{LL}}{(T_F - T_A)_{UL} - (T_F - T_A)} \quad [\text{Equation 6}]$$

The water stress map generated by the CWSI was validated by making comparisons with soil moisture information obtained with EC-5 sensors (Figure 3). The experimental bench was separated into three treatments, each subjected to its irrigation regime, with different water conditions.

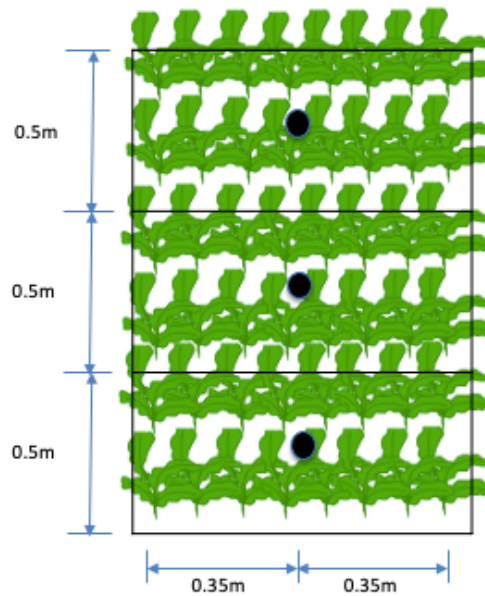


Figure 3 - Distribution of soil moisture sensors placed in the center between the rows of each treatment in the experimental area.

Soil moisture close to the condition of field capacity (CC) was determined before seedling transplanting, saturating the local soil, and monitoring the moisture until it reached a stable value. From the CC information, water stress levels were differentiated in 3 treatments in which irrigation was performed whenever the moisture got a critical value corresponding to T1=85% CC; T2=75%CC; T3=55% CC. The volume of water applied in each treatment area and each irrigation event was fixed (0.7 L). Thus, for T2 and T3 were conditioned continuous levels of water stress for the plants.

The sensor reading routine considered 20 minutes for each measurement and, thus, the system irrigated each treatment individually when the sensors indicated critical moisture corresponding to each treatment. Irrigation events were also recorded to be related to soil moisture data. Monitoring soil moisture (Figure 4) throughout the crop cycle shows that Treatment 1 had the highest water availability in the soil for the plants, with its CVA varying between 85 and 97% of the field capacity of the medium used. Treatment 2 had moisture values ranging between 75 and 84% of CC, and Treatment 3, in turn, had its CVA between 50 and 70%.

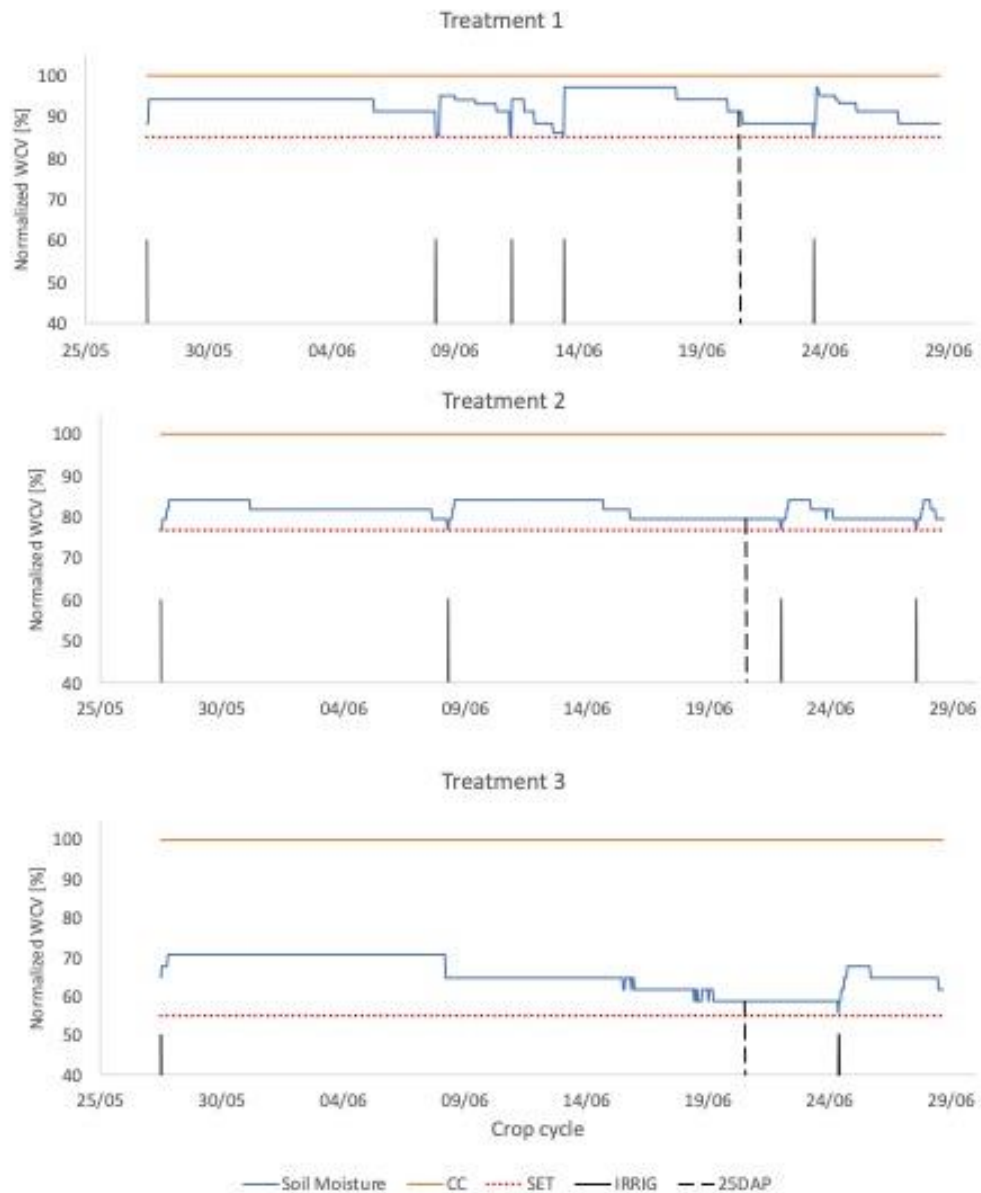


Figure 4 - Moisture Monitoring for each treatment throughout the crop cycle, where the CVA values were normalized to avoid differences in readings between the sensors used.

As they do not present a regular pattern, both the CWSI and the soil moisture were statistically evaluated by the Exponentially Weighted Moving Average (EWMA) chart, as done by [34]).

3. Results

Leaf Temperature Map

The scans performed generated points with local coordinates and the values of T_o , T_A , and RH. But these last two are only used to calculate the CWSI. Figure 5 shows the map generated on the 25th day after planting (DAP), with a complete set of points. Since the scans were daily, a thermal map per day was obtained.

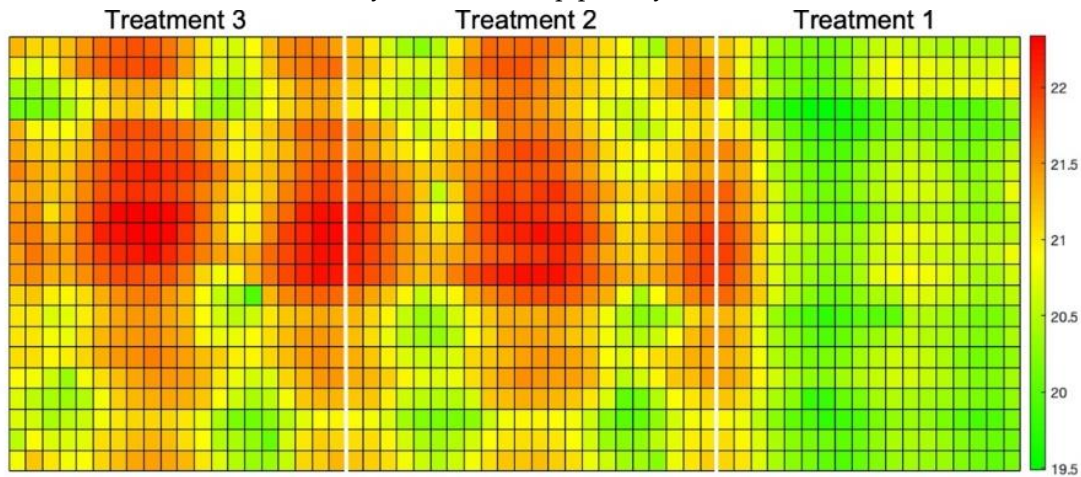


Figure 5- Thermal map of the experimental area, showing points of soil, plant, or a combination of both. The map was generated at 25DAP, the final stage of culture.

It is possible to notice that the observed temperatures vary between 19.5°C and 22.5°C. Still, it is essential to emphasize that points without any plant segmentation were read in this map: pixel readings containing only soil, only plant, and the junction of the two. Points that had only soil presented higher temperatures than the ones with soil and plant or just plant. Only the leaf temperatures must be included for the CWSI calculation to be valid; therefore, the image processing step was performed in the sequence.

Image processing

The 15 images obtained throughout the crop cycle were processed, and a new output image was generated for each of them, that is, a binary image with the segmentation of plants. As the images were captured at different stages of the crop (Figure 6), it was possible to observe different shapes and sizes of the plants and, therefore, evaluate the robustness of the method used.



Figure 6- Images of the crop at different stages of development, used in the evaluation of processing methods.

In addition to the difference between plant density in the experimental area throughout crop development, differences in soil color caused by its moisture are factors that can generate disturbances and affect the results generated in image processing. It is noteworthy that, for this step, there was no division between treatments. By manually classifying the images as a reference in the evaluation of the models, segmented images were generated (Figure 7a).

Subsequently, the pixels with plants received a value of 1 (Figure 7b). Finally, applying the ExG (RGB) equations, it was possible to obtain the model metrics (Table 1), considering the 15 imagens as repetitions.

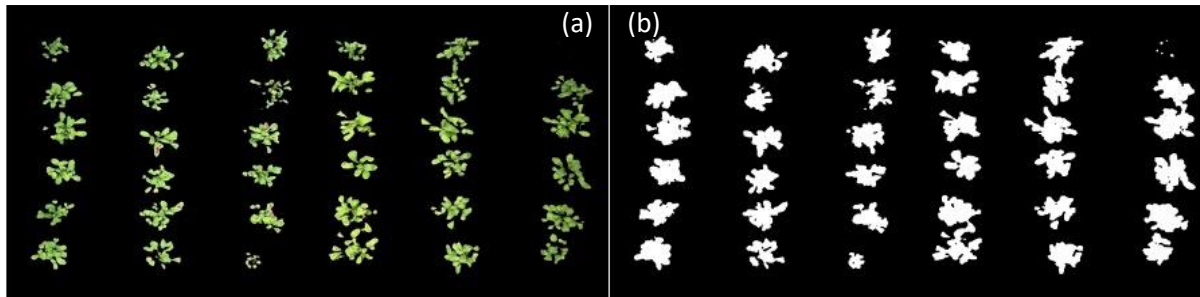


Figure 7- Images used as a reference for evaluating approaches, where (a) the pixels were segmented within the mean of the 10 selected pixels and (b) received a value equal to 1.

Table 1 - Descriptive statistics and ExG(RGB) evaluation metrics for image processing, where N represents the confidence level (95%).

	Precision	Sensitivity	F-Score	Total Error	Accuracy	Processing Time [s]
Mean	88.79%	84.83%	86.54%	9.96%	90.04%	1.50
Standard error	1.28%	1.27%	0.66%	0.58%	0.57%	0.01
Median	89.96%	85.61%	87.14%	9.99%	90.01%	0.50
Standard deviation	5.10%	5.09%	2.65%	2.31%	2.31%	0.03
Sample variance	0.26%	0.26%	0.07%	0.05%	0.05%	0,00
kurtosis	1.76	3.39	1.56	1.97	1.97	-0.81
Skew	-1.26	-1.55	-0.81	-0.09	0.09	-0.50
Interval	19.04%	21.01%	10.80%	10.47%	10.47%	0.10
Minimum	75.29%	70.53%	80.72%	4.54%	84.99%	0.44
Maximum	94.34%	91.54%	91.52%	15.01%	95.46%	0.54
Score	16	16	15	16	15	15
N	2.72%	2.71%	1.41%	1.23%	1.23%	0.02

The F-score was greater than 85%, and the accuracy was close to 90%, indicating an adequate performance of the image segmentation method. The average processing time was 1.5 seconds, indicating a low computational cost. Although this method has relatively low sensitivity values, its precision, that is, the number of pixels classified as plants that were plants, made the total error of the method was less than 10%. The performance of this method corroborated the results of [30], who also indicated the ExG(RGB) with the best *F-score values* in their evaluations. But the processing time found by the author was higher than in this study. This difference is due to the different environmental conditions when the images were captured and show the complexity of image processing, since similar techniques and approaches can produce different results.

With the results of the generated thermal map and the image segmentation, it was possible the crossing of information and the overlap of these data generated an MTF (Figure 8). For this, pixel-by-pixel multiplication of points on the temperature map by values 0 or 1 occurred, according to the processed image.

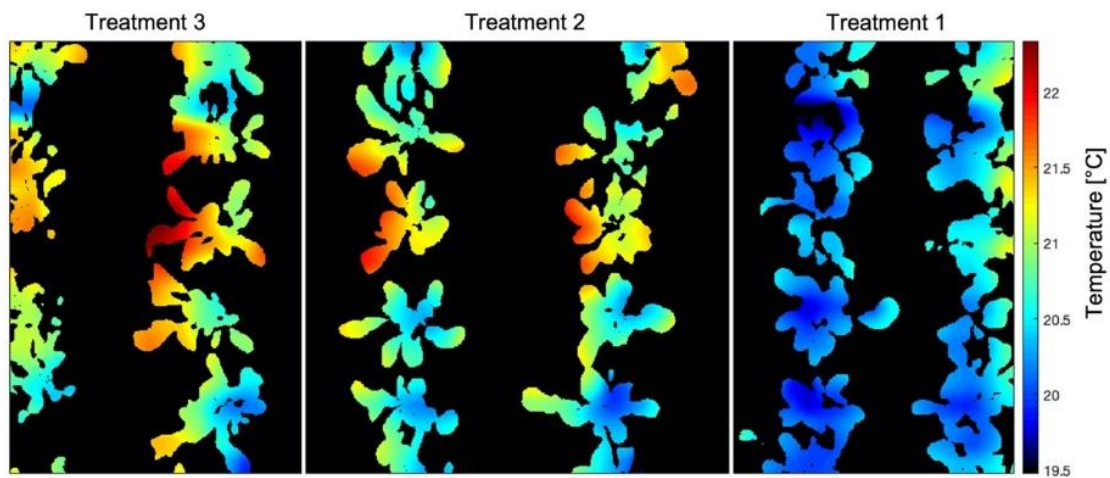


Figure 8 - Leaf Temperature Map generated by crossing the temperature map of the experimental area with the segmented image of the crop - 25DAP

The resizing of the images was essential for overlaying the maps since the RGB image originally had 5000 x 2700 pixels, and the generated temperature map had 61 x 22 pixels, so the final dimensions of the MTF are 1280 x 620 pixels. It can be observed that the treatments presented different ranges of leaf temperatures, where treatment 3, which was irrigated only when the soil CVA reached 55% of CC, had the highest T_f compared to treatments 1 and 2, irrigated in 85% and 75% of CC, respectively. This behavior is expected since the water conditions of each of the treatments are different, causing less water to be available for the plants and, consequently, different levels of stomatal closure.

The validation of the MTF was done through the image obtained by the thermal camera (Figure 9a), where it is possible to identify that the minimum temperatures were 19.2°C. The generated image exceeds the limits of the experimental area, causing the upper range of temperature values to be outside the maximum temperature range of the crop. The plant segmentation image was also superimposed on the thermal image to eliminate the part that does not correspond to the area of interest. Only pixels with plants were evaluated.

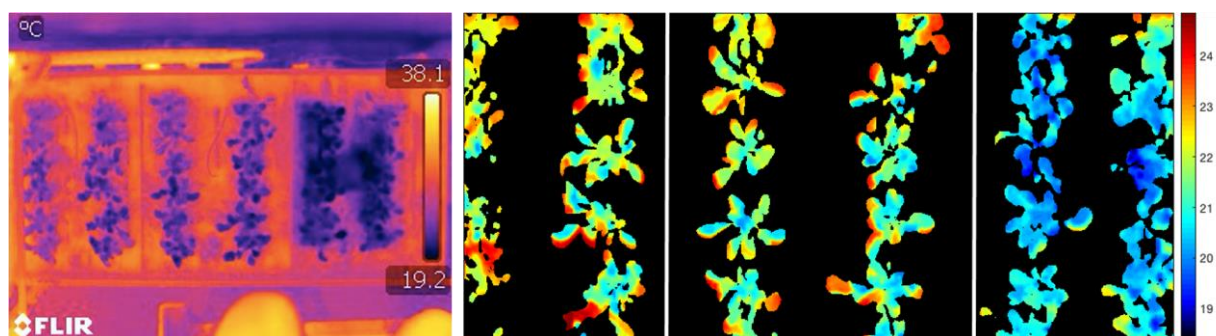


Figure 9 – Generated thermal image, at 25DAP, by the (a) original and (b) resized IR camera with the overlay of the processed image for segmentation of the plants.

The mean error between temperatures measured by the IR sensor and the camera was -0.1959; that is, the temperatures measured by the sensor were, on the mean, 0.2°C below the temperature measured by the thermal camera. The standard error was equal to 0.03%. This sensor is widely used in agricultural studies due to its low cost and the good results presented by [35–38]. Despite the mean error found of 0.2°C being within the precision provided by the

manufacturer, of $\pm 0.5^{\circ}\text{C}$, it can be observed that the scale of values obtained by the thermal camera has points with up to 2.5°C of sensor difference. This difference can be explained by the resizing of maps and images. The interpolation is done in a bilinearized way and by the difference in the number of original pixels. Therefore, the value of the resized pixels may have been changed.

NWSB Equation

The equation was parameterized with $(T_F - T_A)$ values and VPD values measured every 10 minutes throughout the crop cycle on the bench under the same conditions as the bench used for the scans. Figure 10 shows the monitoring of T_O , T_A , and RH, where it can be seen that the temperatures did not have significant variation.

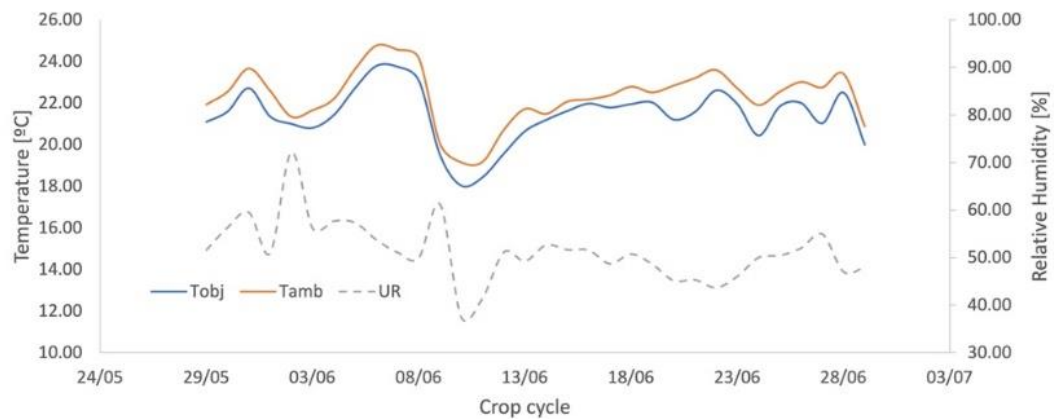


Figure 10 - Ambient and Object Temperature monitoring and Relative Humidity for the auxiliary bench in NWSB parameterization.

When evaluating it, it can be observed that leaf temperature values were consistently below ambient temperatures, which satisfies the equation's parameterization condition, which only foresees plants without water stress. The correlation between temperature difference and VPD (Figure 11) resulted in the equation $(T_F - T_A) = -0,7824 \times VPD + 0,1025$.

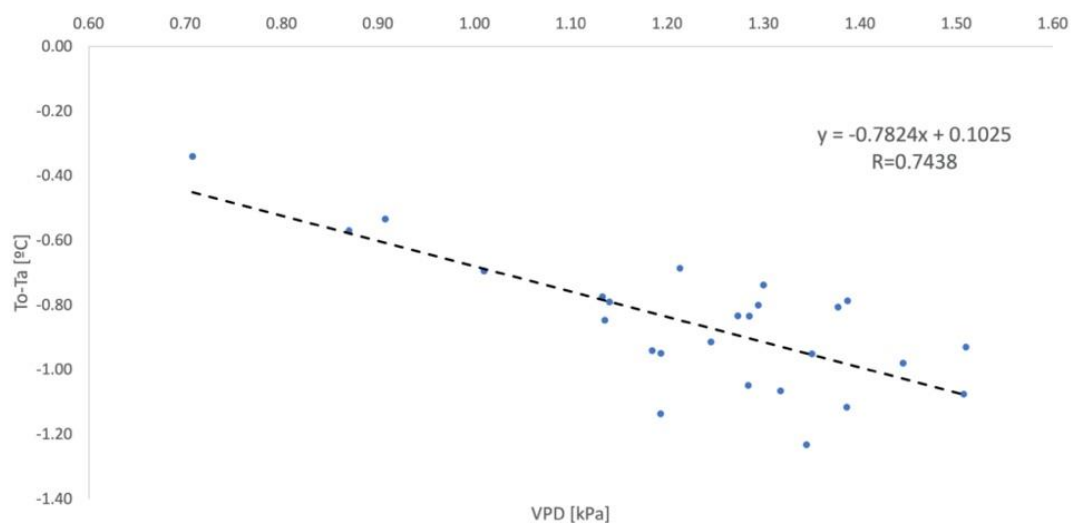


Figure 11- Non-Water-Stressed Baseline Parameterization defined for the protected environment (NWSB_P)

An equation was also parameterized considering an unprotected environment for evaluation purposes, whose monitoring of ambient and leaf temperatures and RH is shown in Figure 12.

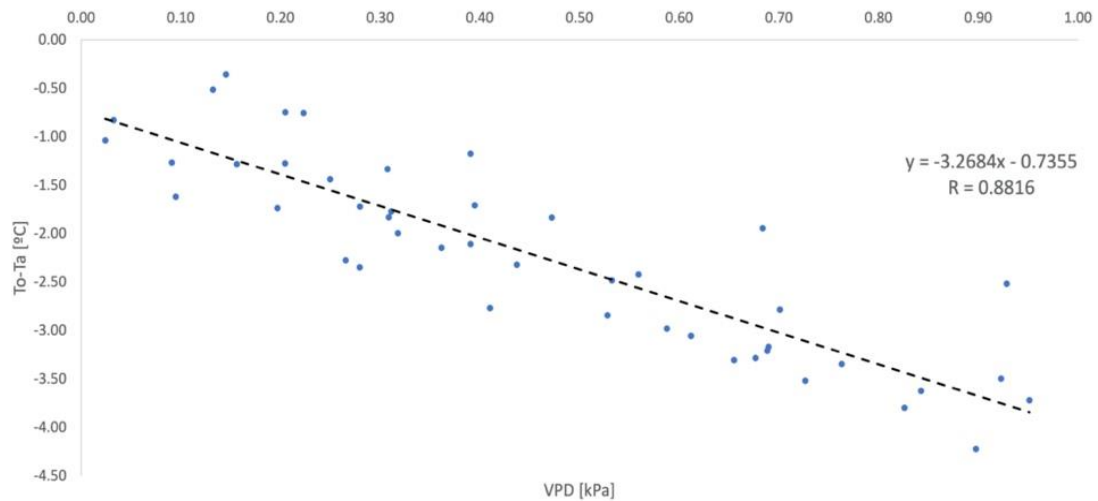


Figure 12 - Non-Water-Stressed Baseline Parameterization defined for the unprotected environment (NWSB_D)

Although the angular coefficients of NWSB_D are in the range of values close to those found in the literature for other crops (Table 2), it was observed that the calculated limits $(T_F - T_A)_{LL}$ and $(T_F - T_A)_{UL}$ did not represent the real relationship between the difference in leaf and ambient temperatures and the VPD, since the experimental bench was in a protected cultivation environment, without the presence of factors such as wind, dew and large variations in temperature. The NWSB_P coefficients were shown to be smaller than those found in parameterizations of other crops.

Table 2 - Non- Water-Stressed Baselines obtained in the literature for different crops

Authors	Crop	NWSB
[9]	Lettuce	$Y = -2.96x + 4.18$
[16]	Watermelon	$Y = -1.20x + 0.47$
[17]	Maize	$Y = -2.81x - 1.35$
[28]	Grape	$Y = -1.71x + 2.54$
[39]	Mustard	$Y = -1.71x - 0.47$

[40] obtained as angular and linear coefficients the values -0.35 and 2.08, respectively. They concluded that a lower angular coefficient is observed in plants with a more dependent relationship with the atmosphere and climate, as is the case of olive trees, which have a low temperature variation for significant variations in the VPD [41]. Furthermore, the authors pointed out the small size of the leaves concerning the tree canopy and even that, for several crops, a certain level of stomatal closure is ordinary when there is an increase in the evaporative demand of the plant.

Wind speed and solar radiation are two parameters that directly influence the achievement of temperature limits, as they change the behavior of plants about their transpiration [42–45]. This evidences that the parameterization of the NWSB must occur under the same climatic conditions in which the CWSI will be calculated [44]. The parameterization must happen that way so that the normalization of temperatures does not occur in a displaced way, causing the lower and upper limits of $(T_F - T_A)$ are outside the actual range of temperature variation.

[5,46] also stated that the shape and size of the leaves could affect the angular and linear coefficients of the NWSB, something relevant in this work since the data were collected every 10 minutes throughout the entire crop cycle. Due to different water requirements, the plant development stage also affects these coefficients [9]. In the literature, some studies collected data for 2 years in pistachio crops [32]. Still, in addition to being large plants, their productive age can reach 25 years [47], or that is, the leaves' physical variations were not significant to affect the NWSB regression. Other works parameterized the equation with data collected for only 3 days, at specific times (8:30 am; 11:30 am; 2:30 pm; 5:30

pm; 8:00 pm)[10], and it was observed that temperature variations in times before 9:00 am and after 4:00 pm do not show good relations with the VPD.

The low slope of the $NWSB_P$ straight line and the dispersion of points show that Arugula can be a crop that presents a small range of differences between T_F and T_A concerning the environment, corroborating the results found by [40]. As a result, the CWSI may be more sensitive to temperature variations since the normalization of temperatures can be affected by the maximum and minimum limits found by $NWSB$. Figure 13 shows that the behavior of the parameterized equations for the two environments was adequate since there is no bias between the variables and the mean of the residuals was equal to zero [48].

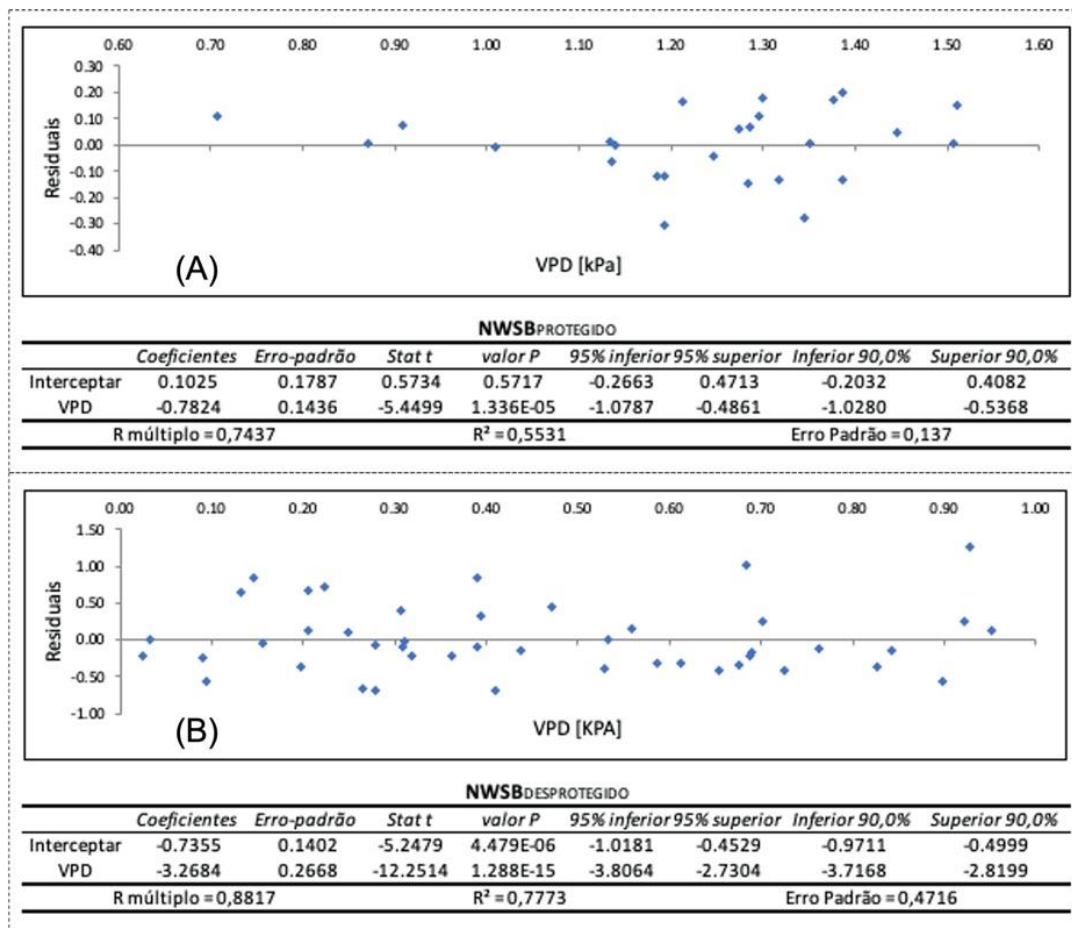


Figure 13 - Regression and Residual Analysis for NWSB parameterized in environments (a) Protected and (b) Unprotected.

CWSI

By calculating the CWSI using the leaf temperature values obtained from the MTF, T_A , and RH obtained by the AM2302 sensor and the limits of the $NWSB_P$ parameterized for the protected environment conditions, it was possible to generate a stress map (Figure 14) in the treatments of the experimental area.

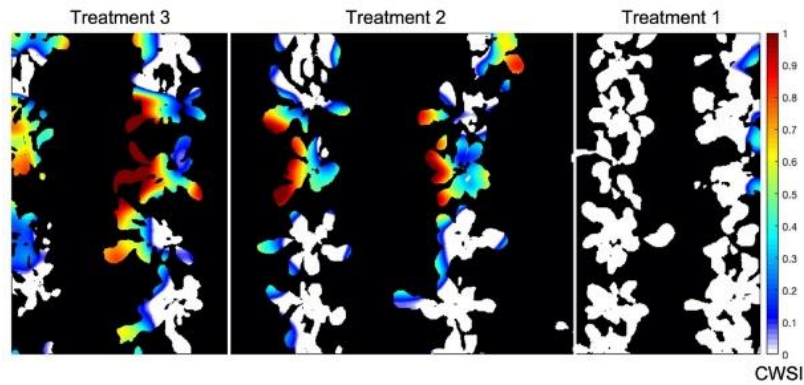


Figure 14 - CWSI map of the experimental area in a protected environment generated for the 25DAP, in a scan carried out at 12:00 pm, the time with the best reading results.

As expected, the behavior of the crop about the environment affected the limits $(T_F - T_A)_{UL}$ and $(T_F - T_A)_{LL}$ obtained from the NWSB equation, causing the CWSI calculation to present values slightly higher than 1. And this would indicate that the plants were under 100% water stress. Still, these characteristics were not verified when visually evaluating the state of the leaves at the points that presented these values, showing that the temperature normalization range was displaced concerning the actual leaf temperatures of the crop. Some negative values were also found, indicating that the plants were not under any water stress, and indirectly, this occurs when the canopy vapor transport resistance (r_a) is lower than the aerodynamic resistance of the air (r_c), as stated by [49].

The calculation of CWSI using the limits coming from NWSB in tropical climates is affected by the high presence of clouds since they affect the solar radiation incident on the crop [7,20]. And the fact that the experimental bench was located in a protected environment, where the plants did not directly receive solar radiation throughout the day, possibly affected the normalized temperature range. CWSI values less than 0 and greater than 1 are reported in the works of [49–51]. As the values obtained were close to the limit normalized by the index, a correction was made so that negative values received 0 as their new value and values greater than 1 were reduced to the CWSI limit. When calculating the CWSI using the limits obtained by the NWSB_D, it was possible to identify that the normalization of $(T_F - T_A)$ values was significantly displaced concerning the actual range of temperature variations. The CWSI map of the crop (Figure 15) generated for the unprotected environment showed high values compared to the map developed for the experimental bench environment. It can be seen that the plants from treatment 1 had CWSI values close to 0.8, while in the map in Figure 14, their values were almost all zero.

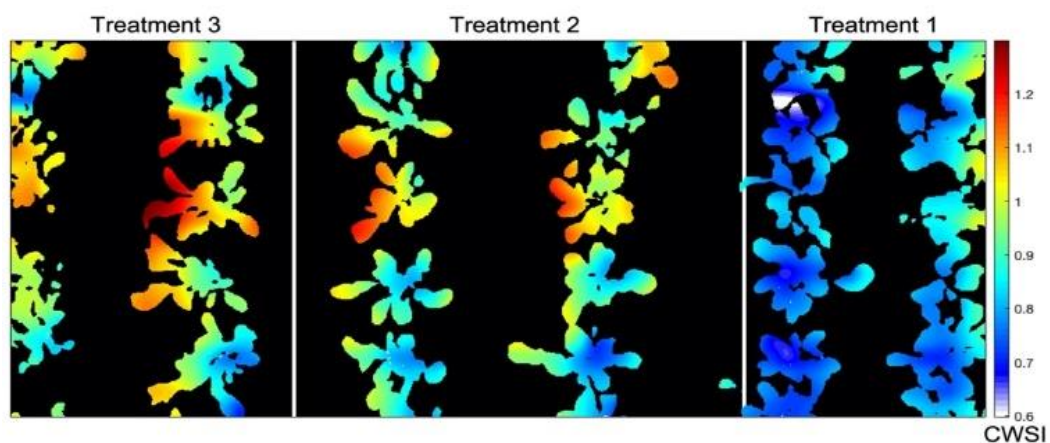


Figure 15 - CWSI map of the experimental area in an unprotected environment generated for 25DAP. The upper and lower limits of NWSB_D did not indicate actual temperature values, and the minimum calculated CWSI was 0.6, corresponding to the situation without water stress.

Just for evaluation purposes, the empirical method was also calculated at 25DAP to find the T_{UL} and T_{LL} limits, following the [13]. One of the leaves was wetted with water 1 minute before the temperature reading, serving as a reference for a surface with maximum transpiration and revealing the minimum temperature that the plant would reach, 19,3°C. The other leaf, covered with vaseline about 30 minutes before the reading, served as a surface where there is no transpiration, indicating as 24,2°C the maximum temperature that the plant could reach under the climatic conditions of the day, presenting $T_A=22,1^\circ\text{C}$ and $RH=47\%$ at the time of measurement. The generated CWSI map (Figure 16) shows that the values did not exceed the limits between 0 and 1 of the index and that the maximum stress level read was 0.45, while the map generated through $NWSB_P$ presented values equal to 1. At the same time, it can be observed that in treatment 1, the CWSI values were between 0,1 and 0,3, whereas in Figure 14, the vast majority of pixels identified as plants had values equal to 0.

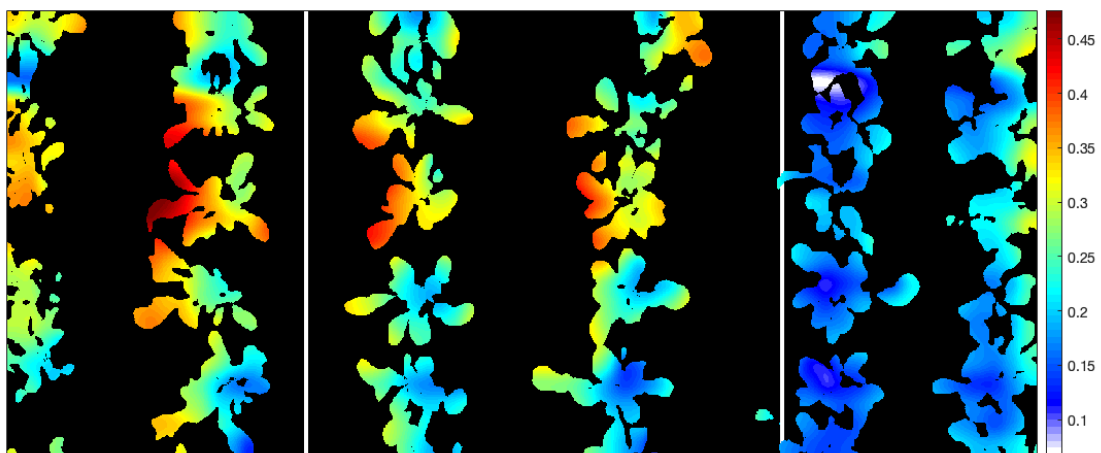


Figure 16 - CWSI map generated for 25DAP, using the empirical method to obtain the T_{MAX} and T_{MIN} through natural reference surfaces. One of the leaves was wetted with water to simulate 100% transpiration and the other with vaseline to block leaf transpiration.

Although the use of natural reference surfaces for the determination of temperature limits results in a range of CWSI values more minor than those presented by the protected environment equation, the use of this methodology makes it difficult to process automation because it requires surfaces for all scans that are made of the tillage area. [28] studied remote thermal sensing to calculate the CWSI and compared it with local methods of measuring leaf water potential (ψ_L) for viticulture. Their results confirmed existing consensus in the literature that there is a direct relationship between ψ_L and the CWSI, as shown in Table 3. Furthermore, the authors concluded that the value of 0.2 should be used to define an irrigation regime on based on CWSI.

Table 3 -Index values – adapted from BELVERT et al. (2014)

Stress Level	ψ_L [MPa]	CWSI
Well irrigated vines	$-0.8 \leq \psi_L \leq -0.6$	$CWSI \leq 0.2$
Vines under moderate stress	$-1.0 \leq \psi_L \leq -1.2$	$0.3 \leq CWSI \leq 0.5$
Vines under severe stress	$\psi_L \leq -1.5$	$0.7 \leq CWSI$

When correlating the CWSI with the productivity in the eggplant crop, [12] also obtained the best results for index values equal to 0.2, noting the productivity to fall from 78.7 to 40.9 t ha⁻¹ when the CWSI increased to 0.6. As for

the watermelon crop, the productivity of treatments with the indices 0.2 and 0.4 and 0.6 showed no statistical differences, showing that the crop resists higher levels of water stress without harming its development. Therefore, an irrigation system based on CWSI equal to 0.6 could have better water use, reducing its consumption [16].

At 25DAP, the date on which the maps presented in this work were generated, CWSI mean values were 0.0072, 0.2731, and 0.3840 for treatments 1, 2, and 3, respectively. Already the values moisture showed 91.21%CC, 79.50%CC, and 58.80%CC. Thus, throughout the entire crop cycle (Figure 17), it was possible to observe that the stress levels increased when the soil moisture of each treatment decreased, revealing that the proposed system could detect the water stress caused by different water conditions.

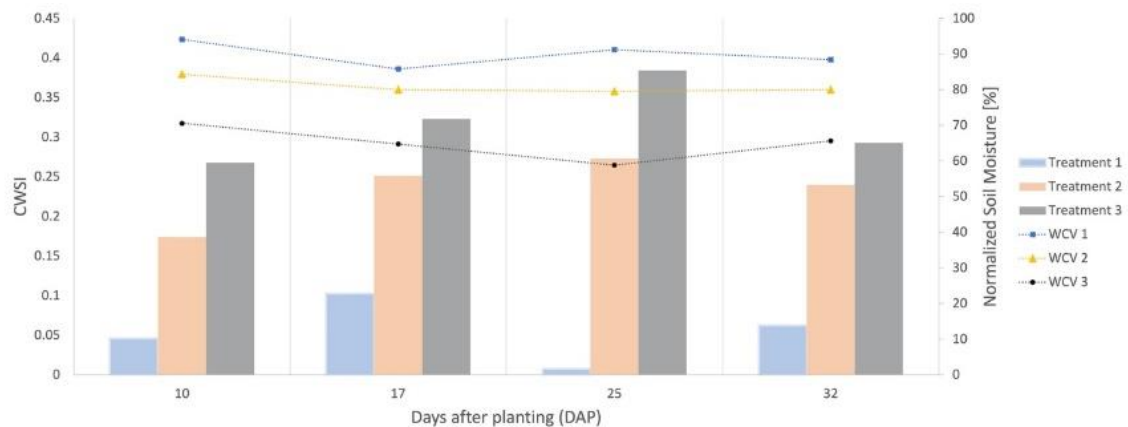


Figure 17 - Levels of water stress throughout the entire Arugula cycle. Soil moisture was normalized by the field capacity of each treatment, thus equaling the references used for measurement.

The above results indicate that one of the plant's responses to reducing water availability is increase leaf temperature caused by stomatal closure [42]. Thus, the CWSI is a good indicator of water stress. It can be used to define the irrigation management of individual plants or areas with the same treatment, corroborating the results obtained by [14,17,52], who defined irrigation management using a CWSI limit value for different crops. These values vary according to the stage of crop development [53], revealing the importance of monitoring stress levels throughout the entire plant cycle.

As discussed by [54], the use of this methodology requires the measurement of simple parameters such as plant and air temperatures and relative humidity, dispensing with the help of complex instruments or sensors. By analyzing the EWMA charts (Figure 18), it was possible to observe that none of the points selected throughout the crop cycle were outside the upper (LSC) and lower (LIC) control limits, indicating the stability of the process and corroborating the results obtained by [34,55]. If any of the points were out of limits, the process should be considered unstable.

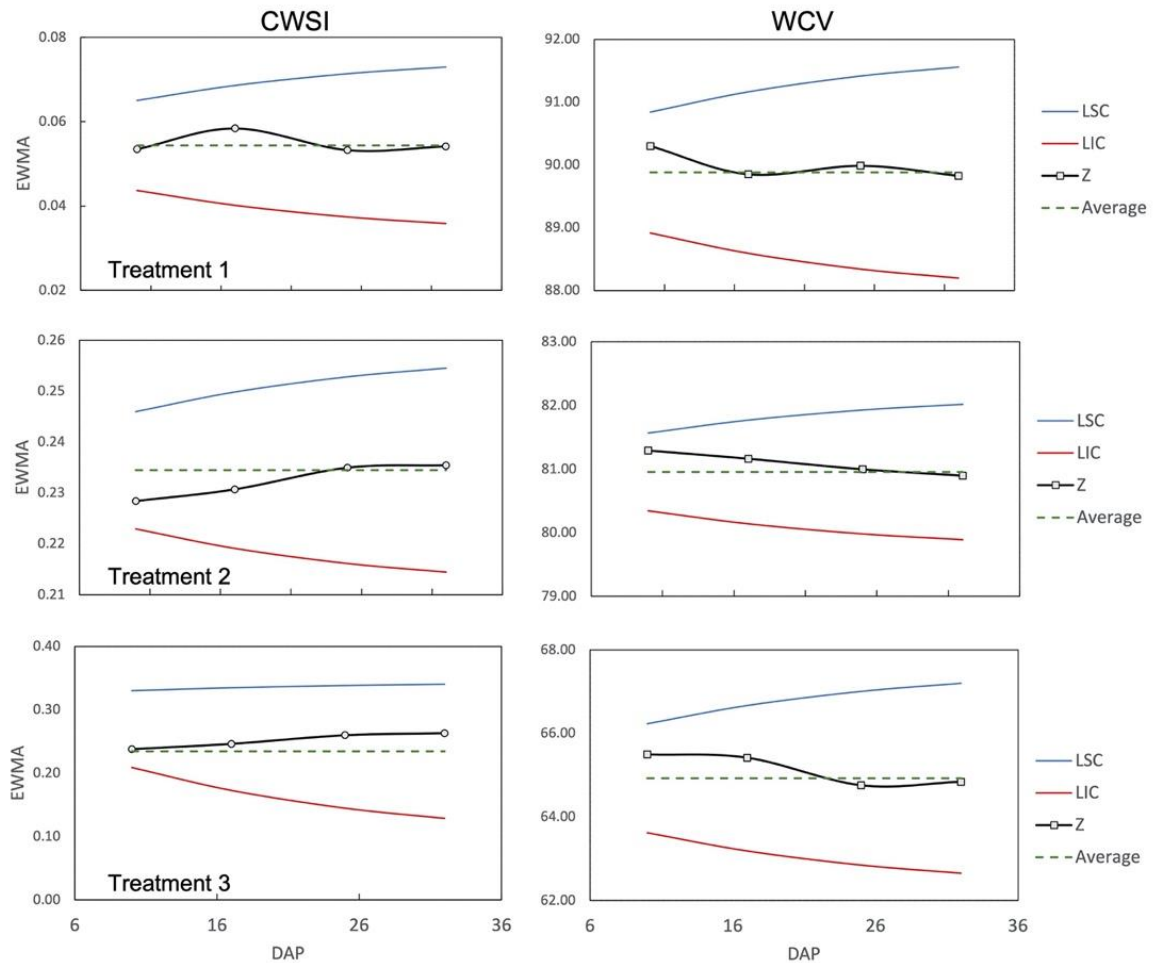


Figure 18 -Charts of the exponentially weighted moving average of the CWSI and CVA for each treatment.

5. Conclusions

It has been demonstrated that it is possible to use low-cost IR sensors with directional FOV to measure plant temperature, generate thermal maps and identify water stress conditions. The Leaf Temperature Maps, generated by the IR sensor readings the plant segmentation in the RGB image, were validated by thermal images.

The ExG(RGB) method, used for the segmentation of RGB images, showed good classification metrics, between 86 to 90% of correct classifications, and low computational cost, reducing the need for high-performance computers and enabling the use of embedded devices. The parameterization of NWSB showed that the plant responds in different ways in different climatic conditions.

The proposed system detected different CWSI values for soil moisture variations since the stress index increased with the reduction of water availability. However, the EWMA charts showed the stability of the process. The results achieved in this work suggest and allow future studies for the creation of a control system based on the CWSI to define the irrigation management in an automated irrigation system.

Author Contributions: Conceptualization, Rodrigo Leme de Paula, Angel Pontin Garcia, Daniel Albiero; Methodology, Rodrigo Leme de Paulo, Angel Pontin Garcia; validation, Rodrigo Leme de Paulo, Fabricio Theodoro Soares; Formal analysis, Rodrigo Leme de Paulo, Antonio Pires de Camargo, Daniel Albiero; investigation, Rodrigo Leme de Paulo; resources, Daniel Albiero; data curation, Rodrigo Leme de Paulo, Claudio Kijyoshi Umezu; writing—original draft preparation,

Rodrigo Leme de Paulo; writing—review and editing, Daniel Albiero; Claudio Kiyoshi Umezu ; project administration, Angel Pontin Garcia; funding acquisition, Daniel Albiero. All authors have read and agreed to the published version of the manuscript.

Funding: This research was funded by FAPESP, award number 19/06078-8; by FUNDEP-Rota 2030, award number 27192.03.01/2020.13-00

Data Availability Statement: Not applicable.

Acknowledgments: This study was financed in part by the Coordination for the Improvement of Higher Education Personnel – Brazil (CAPES) – Finance Code 001 through the first author’s scholarship. The last author thanks CNPq for the productivity grant (303331/2021-6).

Conflicts of Interest: The authors declare no conflict of interest.

References

1. RASSINI, J.B. Manejo Da Água de Irrigação. In *Irrigação e fertilização em fruteiras e hortaliças*; 2011; pp. 156–232.
2. Albiero, D. Agricultural Robotics: A Promising Challenge. *Current Agriculture Research Journal* **2019**, *7*, 01–03, doi:10.12944/CARJ.7.1.01.
3. Albiero, D. Robots and AI: Illusions and Social Dilemmas. **2022**, doi:10.1007/978-3-030-95790-2.
4. Abioye, E.A.; Abidin, M.S.Z.; Mahmud, M.S.A.; Buyamin, S.; Ishak, M.H.I.; Rahman, M.K.I.A.; Otuoze, A.O.; Onotu, P.; Ramli, M.S.A. A Review on Monitoring and Advanced Control Strategies for Precision Irrigation. *Comput Electron Agric* **2020**, *173*, 105441, doi:10.1016/j.compag.2020.105441.
5. Xavier, R.S.; Galvão, C.B.; Rodrigues, R.L.; Garcia, A.P.; Albiero, D.; Xavier, R.S.; Galvão, C.B.; Rodrigues, R.L.; Garcia, A.P.; Albiero, D. Mechanical Properties of Lettuce (*Lactuca Sativa* L.) for Horticultural Machinery Design. *Sci Agric* **2022**, *79*, 2022, doi:10.1590/1678-992X-2020-0249.
6. Kacira, M.; Ling, P.P.; Short, T.H. ESTABLISHING CROP WATER STRESS INDEX (CWSI) THRESHOLD VALUES FOR EARLY, NON-CONTACT DETECTION OF PLANT WATER STRESS. *Transactions of the ASAE* **2002**, *45*, 775–780.
7. Costa, J.M.; Grant, O.M.; Chaves, M.M. Thermography to Explore Plant-Environment Interactions. *J Exp Bot* **2013**, *64*, 3937–3949, doi:10.1093/jxb/ert029.
8. Albiero, D.; Pontin Garcia, A.; Kiyoshi Umezu, C.; Leme de Paulo, R. Swarm Robots in Mechanized Agricultural Operations: A Review about Challenges for Research. *Comput Electron Agric* **2022**, *193*, 106608, doi:10.1016/J.COMPAG.2021.106608.
9. Idso, S.B. Non-Water-Stressed Baselines: A Key to Measuring and Interpreting Plant Water Stress. *Agricultural Meteorology* **1982**, *27*, 59–70, doi:10.1016/0002-1571(82)90020-6.
10. García-Tejero, I.F.; Rubio, A.E.; Viñuela, I.; Hernández, A.; Gutiérrez-Gordillo, S.; Rodríguez-Pleguezuelo, C.R.; Durán-Zuazo, V.H. Thermal Imaging at Plant Level to Assess the Crop-Water Status in Almond Trees (Cv. Guara) under Deficit Irrigation Strategies. *Agric Water Manag* **2018**, *208*, 176–186, doi:10.1016/j.agwat.2018.06.002.
11. Alsalam, B.H.Y.; Morton, K.; Campbell, D.; Gonzalez, F. Autonomous UAV with Vision Based On-Board Decision Making for Remote Sensing and Precision Agriculture. *IEEE Aerospace Conference Proceedings* **2017**, doi:10.1109/AERO.2017.7943593.
12. Çolak, Y.B.; Yazar, A.; Çolak, İ.; Akça, H.; Duraktekin, G. Evaluation of Crop Water Stress Index (CWSI) for Eggplant under Varying Irrigation Regimes Using Surface and Subsurface Drip Systems. *Agriculture and Agricultural Science Procedia* **2015**, *4*, 372–382, doi:10.1016/j.aaspro.2015.03.042.
13. Camoglu, G.; Demirel, K.; Genc, L. Use of Infrared Thermography and Hyperspectral Data to Detect Effects of Water Stress on Pepper. *Quant Infrared Thermogr J* **2018**, *15*, 81–94, doi:10.1080/17686733.2017.1331008.

14. Ben-Gal, A.; Agam, N.; Alchanatis, V.; Cohen, Y.; Yermiyahu, U.; Zipori, I.; Presnov, E.; Sprintsin, M.; Dag, A. Evaluating Water Stress in Irrigated Olives: Correlation of Soil Water Status, Tree Water Status, and Thermal Imagery. *Irrig Sci* **2009**, *27*, 367–376, doi:10.1007/s00271-009-0150-7.
15. da Silva, C.J.; da Silva, C.A.; de Freitas, C.A.; Golynski, A.; da Silva, L.F.M.; Frizzzone, J.A. Tomato Water Stress Index as a Function of Irrigation Depths. *Revista Brasileira de Engenharia Agrícola e Ambiental* **2018**, *22*, 95–100, doi:10.1590/1807-1929/agriambi.v22n2p95-100.
16. Erdem, Y.; Erdem, T.; Orta, A.H.; Okursoy, H. Irrigation Scheduling for Watermelon With Crop Water Stress Index (Cwsi). *Journal of Central European Agriculture* **2006**, *6*, 449–460, doi:10.5513/jcea.v6i4.322.
17. Fattahi, K.; Babazadeh, H.; Najafi, P.; Sedghi, H. Scheduling Maize Irrigation Based on Crop Water Stress Index (CWSI). *Appl Ecol Environ Res* **2018**, *16*, 7535–7549, doi:10.15666/aeer/1606_75357549.
18. Ballester, C.; Jiménez-Bello, M.A.; Castel, J.R.; Intrigliolo, D.S. Usefulness of Thermography for Plant Water Stress Detection in Citrus and Persimmon Trees. *Agricultural and Forest Meteorology* **2013**, *168*, 120–129, doi:http://dx.doi.org/10.1016/j.agrformet.2012.08.005.
19. Freitas, C. De; Kalliany, K.; Neto, F.B.; Grangeiro, C.; Silva, J.S. Desempenho Agrônômico de Rúcula Sob Diferentes Espaçamentos e Agronomic Performance of Rocket under Different Spacing and Planting Times Material e Métodos Dois Experimentos Foram Conduzidos Na Horta Do. *Revista Ciência Agrônômica* **2009**, *40*, 449–454.
20. Adeyemi, O.; Grove, I.; Peets, S.; Domun, Y.; Norton, T. Dynamic Modelling of the Baseline Temperatures for Computation of the Crop Water Stress Index (CWSI) of a Greenhouse Cultivated Lettuce Crop. *Comput Electron Agric* **2018**, *153*, 102–114, doi:10.1016/j.compag.2018.08.009.
21. SHIRMOHAMMADI, A.Z.; KAMGRA, H.A.A.; SEPASKHAH, A.R. Use of Crop Water Stress Index (CWSI) for Evaluation of Water Status and Irrigation Scheduling of Saffron. *Iranian Journal of Horticultural Science and Technology* **2006**, *7*, 23–32.
22. Monteith, J.L.; Unsworth, M.H. *Principles of Environmental Physics*; Fourth.; Elsevier / Academic Press, 2013; ISBN 9780123869937.
23. Jones, H.G.; Hutchinson, P.A.; May, T.; Jamali, H.; Deery, D.M. A Practical Method Using a Network of Fixed Infrared Sensors for Estimating Crop Canopy Conductance and Evaporation Rate. *Biosyst Eng* **2018**, *165*, 59–69, doi:10.1016/j.biosystemseng.2017.09.012.
24. Garcia, A.P.; Umez, C.K.; Polania, E.C.M.; Dias Neto, A.F.; Rossetto, R.; Albiero, D. Sensor-Based Technologies in Sugarcane Agriculture. *Sugar Tech* **2022**, *24*, 679–698, doi:10.1007/S12355-022-01115-5/FIGURES/7.
25. Muangprathub, J.; Boonnam, N.; Kajornkasirat, S.; Lekbangpong, N.; Wanichsombat, A.; Nillaor, P. IoT and Agriculture Data Analysis for Smart Farm. *Comput Electron Agric* **2019**, *156*, 467–474, doi:10.1016/j.compag.2018.12.011.
26. Mesas-Carrascosa, F.J.; Verdú Santano, D.; Meroño, J.E.; Sánchez de la Orden, M.; García-Ferrer, A. Open Source Hardware to Monitor Environmental Parameters in Precision Agriculture. *Biosyst Eng* **2015**, *137*, 73–83, doi:10.1016/j.biosystemseng.2015.07.005.
27. Flores, K.O.; Butaslac, I.M.; Gonzales, J.E.M.; Dumlao, S.M.G.; Reyes, R.S.J. Precision Agriculture Monitoring System Using Wireless Sensor Network and Raspberry Pi Local Server. *IEEE Region 10 Annual International Conference, Proceedings/TENCON* **2017**, 3018–3021, doi:10.1109/TENCON.2016.7848600.
28. Bellvert, J.; Zarco-Tejada, P.J.; Girona, J.; Fereres, E. Mapping Crop Water Stress Index in a ‘Pinot-Noir’ Vineyard: Comparing Ground Measurements with Thermal Remote Sensing Imagery from an Unmanned Aerial Vehicle. *Precis Agric* **2013**, *15*, 361–376, doi:10.1007/s11119-013-9334-5.

29. Woebbecke, D.M.; Meyer, G.E.; Von Bargen, K.; Mortensen, D.A. Color Indices for Weed Identification under Various Soil, Residue, and Lighting Conditions. *Transactions of the American Society of Agricultural Engineers* **1995**, *38*, 259–269, doi:10.13031/2013.27838.
30. Perissini, I.C. Análise Experimental de Algoritmos de Constância de Cor e Segmentação Para Detecção de Mudanças de Plantas. **2018**.
31. Bailly, S.; Giordano, S.; Landrieu, L.; Chehata, N. Crop-Rotation Structured Classification Using Multi-Source Sentinel Images and LPIS for Crop Type Mapping. *International Geoscience and Remote Sensing Symposium (IGARSS)* **2018**, 2018-July, 1950–1953, doi:10.1109/IGARSS.2018.8518427.
32. Testi, L.; Goldhamer, D.A.; Iniesta, F.; Salinas, M. Crop Water Stress Index Is a Sensitive Water Stress Indicator in Pistachio Trees. *Irrig Sci* **2008**, *26*, 395–405, doi:10.1007/s00271-008-0104-5.
33. Idso, S.B.; Jackson, R.D.; Pinter, P.J.; Reginato, R.J.; Hatfield, J.L. Normalizing the Stress-Degree-Day Parameter for Environmental Variability. *Agricultural Meteorology* **1981**, *24*, 45–55, doi:10.1016/0002-1571(81)90032-7.
34. Albiero, D.; Maciel, A.J. da S.; Milan, M.; Monteiro, L. de A.; Mion, R.L. Avaliação Da Distribuição de Sementes Por Uma Semeadora de Anel Interno Rotativo Utilizando Média Móvel Exponencial. *Revista Ciência Agronômica* **2012**, *43*, 86–95, doi:10.1590/s1806-66902012000100011.
35. Sudianto, A.; Jamaludin, Z.; Abdul Rahman, A.A.; Novianto, S.; Muharrom, F. Smart Temperature Measurement System for Milling Process Application Based on MLX90614 Infrared Thermometer Sensor with Arduino. *Journal of Advanced Research in Applied Mechanics* **2020**, *72*, 10–24, doi:10.37934/aram.72.1.1024.
36. Martínez, J.; Egea, G.; Agüera, J.; Pérez-Ruiz, M. A Cost-Effective Canopy Temperature Measurement System for Precision Agriculture: A Case Study on Sugar Beet. *Precis Agric* **2017**, *18*, 95–110, doi:10.1007/s11119-016-9470-9.
37. Fisher, D.K.; Kebede, H. A Low-Cost Microcontroller-Based System to Monitor Crop Temperature and Water Status. *Comput Electron Agric* **2010**, *74*, 168–173, doi:10.1016/j.compag.2010.07.006.
38. Gintsioudis, I.; Skoufogianni, E.; Bartzialis, D.; Giannoulis, K.; Danalatos, N. Diurnal Variations in Leaf – Air Temperature and Vapor Pressure Deficit of Sunlit and Shaded Kenaf Leaves. *CEUR Workshop Proc* **2020**, 2761, 574–579.
39. Kumar, N.; Poddar, A.; Shankar, V.; Ojha, C.S.P.; Adeloye, A.J. Crop Water Stress Index for Scheduling Irrigation of Indian Mustard (*Brassica Juncea*) Based on Water Use Efficiency Considerations. *J Agron Crop Sci* **2020**, *206*, 148–159, doi:10.1111/jac.12371.
40. Berni, J.A.J.; Zarco-Tejada, P.J.; Sepulcre-Cantó, G.; Fereres, E.; Villalobos, F. Mapping Canopy Conductance and CWSI in Olive Orchards Using High Resolution Thermal Remote Sensing Imagery. *Remote Sens Environ* **2009**, *113*, 2380–2388, doi:10.1016/j.rse.2009.06.018.
41. Agam, N.; Cohen, Y.; Berni, J.A.J.; Alchanatis, V.; Kool, D.; Dag, A.; Yermiyahu, U.; Ben-Gal, A. An Insight to the Performance of Crop Water Stress Index for Olive Trees. *Agric Water Manag* **2013**, *118*, 79–86, doi:10.1016/j.agwat.2012.12.004.
42. Jackson, R.D.; Idso, S.B.; Reginato, R.J.; Pinter, P.J. Canopy Temperature as a Crop Water Stress Indicator. *Water Resour Res* **1981**, *17*, 1133–1138, doi:10.1029/WR017i004p01133.
43. Rud, R.; Cohen, Y.; Alchanatis, V.; Levi, A.; Brikman, R.; Shenderoy, C.; Heuer, B.; Markovitch, T.; Dar, Z.; Rosen, C.; et al. Crop Water Stress Index Derived from Multi-Year Ground and Aerial Thermal Images as an Indicator of Potato Water Status. *Precis Agric* **2014**, *15*, 273–289, doi:10.1007/s11119-014-9351-z.
44. Jackson, R.D.; Kustas, W.P.; Choudhury, B.J. A Reexamination of the Crop Water Stress Index. *Irrig Sci* **1988**, *9*, 309–317, doi:10.1007/BF00296705.

45. Wang, X.; Yang, W.; Wheaton, A.; Cooley, N.; Moran, B. Automated Canopy Temperature Estimation via Infrared Thermography: A First Step towards Automated Plant Water Stress Monitoring. *Comput Electron Agric* **2010**, *73*, 74–83, doi:10.1016/j.compag.2010.04.007.
46. Idso, S.B.; Reginato, R.J.; Clawson, K.L.; Anderson, M.G. On the Stability of Non-Water-Stressed Baselines. *Agric For Meteorol* **1984**, *32*, 177–182.
47. Gilman, K.L. Pistachio Yields and Nut Quality Determination and the Relationship Between Soil Characteristics, California State University, 2021.
48. Vogt, H.H.; de Melo, R.R.; Daher, S.; Schmuelling, B.; Antunes, F.L.M.; dos Santos, P.A.; Albiero, D. Electric Tractor System for Family Farming: Increased Autonomy and Economic Feasibility for an Energy Transition. *J Energy Storage* **2021**, *40*, 102744, doi:10.1016/J.EST.2021.102744.
49. Barbosa Da Silva, B.; Ramana Rao, T. V. The CWSI Variations of a Cotton Crop in a Semi-Arid Region of Northeast Brazil. *J Arid Environ* **2005**, *62*, 649–659, doi:10.1016/j.jaridenv.2005.01.017.
50. Hernández-Clemente, R.; Hornero, A.; Mottus, M.; Penuelas, J.; González-Dugo, V.; Jiménez, J.C.; Suárez, L.; Alonso, L.; Zarco-Tejada, P.J. Early Diagnosis of Vegetation Health From High-Resolution Hyperspectral and Thermal Imagery: Lessons Learned From Empirical Relationships and Radiative Transfer Modelling. *Current Forestry Reports* **2019**, *5*, 169–183, doi:10.1007/s40725-019-00096-1.
51. Quebrajo, L.; Perez-Ruiz, M.; Pérez-Urrestarazu, L.; Martínez, G.; Egea, G. Linking Thermal Imaging and Soil Remote Sensing to Enhance Irrigation Management of Sugar Beet. *Biosyst Eng* **2018**, *165*, 77–87, doi:10.1016/j.biosystemseng.2017.08.013.
52. Ciekowski, W.; Szporak-Wasilewska, S.; Kleniewska, M.L.; Józwiak, J.; Gnatowski, T.; Dabrowski, P.; Góraj, M.; SzatyLowicz, J.; Ignar, S.; Chormański, J.L. Remotely Sensed Land Surface Temperature-Based Water Stress Index for Wetland Habitats. *Remote Sens (Basel)* **2020**, *12*, doi:10.3390/rs12040631.
53. Gontia, N.K.; Tiwari, K.N. Development of Crop Water Stress Index of Wheat Crop for Scheduling Irrigation Using Infrared Thermometry. *Agric Water Manag* **2008**, *95*, 1144–1152, doi:10.1016/j.agwat.2008.04.017.
54. Alchanatis, V.; Cohen, Y.; Cohen, S.; Moller, M.; Sprinstin, M.; Meron, M.; Tsipris, J.; Saranga, Y.; Sela, E. Evaluation of Different Approaches for Estimating and Mapping Crop Water Status in Cotton with Thermal Imaging. *Springer Science+Business Media* **2009**.
55. Holt, C.C. Forecasting Seasonals and Trends by Exponentially Weighted Moving Averages. *Int J Forecast* **2004**, *20*, 5–10, doi:10.1016/j.ijforecast.2003.09.015.